Available online at www.sciencedirect.com
ScienceDirect
Acta Materialia 59 (2011) 5032–5039
Acta MATERIALIA
www.elsevier.com/locate/actamat

Comparison of the optical, thermal and structural properties of Ge–Sb–S thin films deposited using thermal evaporation and pulsed laser deposition techniques

J.D. Musgraves [a,*], N. Carlie [a], J. Hu [b], L. Petit [a], A. Agarwal [b], L.C. Kimerling [b], K.A. Richardson [a]

[a] School of Materials Science and Engineering, Clemson University, Clemson, SC 29634, USA
[b] Materials Processing Center, MIT, Cambridge, MA 02139, USA

Received 17 December 2010; received in revised form 27 April 2011; accepted 28 April 2011
Available online 26 May 2011

Abstract

Thin films of $Ge_{23}Sb_7S_{70}$ glass were prepared by thermal evaporation (TE) and pulsed laser deposition (PLD) techniques. We measured their thermal, optical and structural properties and compared with those of the parent bulk. The probe penetration temperature (T_p) of the bulk glass, measured using a micro-thermal analyzer, was found to be 412 ± 10 °C, while those of the TE and PLD films were 468 and 470 ± 10 °C, respectively. The refractive index of the bulk and thin films was measured by ellipsometry and ultraviolet–visible–near infrared transmission spectroscopy, and we show that the films have similar refractive indices, which are lower than those of the parent bulk glass. Using micro-Raman spectroscopy, the structure of the film was investigated. The films contain homopolar Ge–Ge bonds and a lower number of homopolar S–S bonds compared to bulk material, which leads to an increase in the proportion of corner shared $GeS_{4/2}$ units in the films as compared to the bulk glass. Comparison of structural entities associated with each deposition process showed that the TE film possesses a lower number of S–S bonds and a slightly higher number of $SbS_{3/2}$ units compared to the PLD film. These structural changes lead to a more interconnected glass network, and therefore to a higher viscosity at elevated temperatures, as well as a higher refractive index, presumably through increased density. Post-deposition of annealing of these films causes their thermal and optical properties to revert to a more bulk-like state, suggesting that these property differences are due to a difference in the thermal histories of the bulk and film glass networks. For the first time to our knowledge, the refractive index of the bulk glass in the 0.6–10.6 μm range, measured using the prism coupling technique, is also presented.

Keywords: Micro-thermal analysis; Chalcogenide glass; Thin films; Pulsed laser deposition; Thermal evaporation

1. Introduction

Chalcogenide glasses (ChGs) exhibit interesting properties which can be exploited for the fabrication of photonic devices. In particular, they possess excellent infrared transparency, large linear and nonlinear refractive indices [1], low phonon energies, and properties that are tunable through compositional tailoring. These attributes make ChGs good candidates for near-, mid- and long-wave infrared (IR) applications as compared to oxide glasses and single crystals, despite their often limited thermal and mechanical stability. ChGs have been studied extensively for next-generation fiber applications, such as Raman gain [2], super-continuum generation [3] and use as micro-structured fiber [4] for infrared applications. Development of thin film deposition methods and subsequent characterization of material properties for the glass in planar form

* Corresponding author. Tel.: +1 864 656 1259; fax: +1 864 656 1099.
E-mail address: jdm047@clemson.edu (J.D. Musgraves).

1359-6454/$36.00 © 2011 Acta Materialia Inc. Published by Elsevier Ltd. All rights reserved.
doi:10.1016/j.actamat.2011.04.060

provides further opportunities for use in novel applications, such as planar film-based all-optical switches [5] and integrated optical elements for on-chip-sensor applications [6,7]. The glasses also serve as potential candidates for applications in reversible optical recording, memory switching [8] and all-optical circuits [9], and as integrated optical elements [10]. Recently, our group has been evaluating ChG films for their use in on-chip planar chemical sensors for the detection of near- or mid-IR absorbing chemical species [11].

There are several previously reported methods for preparation of ChG thin films, including: chemical reaction from the vapor phase [12], thermal evaporation (TE) from bulk target materials [13], sol–gel [14], radio-frequency magnetron sputtering [15] and pulsed laser deposition (PLD) [16–18]. The PLD technique involves the use of high-power, short-pulse lasers to ablate the target material, producing a vapor plume which condenses onto a substrate, forming a film. In comparison, thermal evaporation (TE) is a more commonly employed technique, and involves electrical heating of a boat containing the target material within a vacuum chamber at low pressures (typically $\sim 10^{-6}$ torr) to a temperature above its melting point, where vaporization of the target occurs. Once a desired vapor pressure for the target material has been reached, a cooler substrate is exposed and the molecular units from the target material vapor condense on the surface. The physical process and kinetics of the TE and PLD techniques are quite different, and can often produce films with differing structures and thus variations in their optical and thermal properties. An understanding of the process-induced property variation is critical for the design of key optical devices based on such films.

This paper reports the results of physical, optical and structural property analyses of $Ge_{23}Sb_7S_{70}$ thin films deposited via two different deposition routes. Specifically, glassy thin films were prepared via PLD and TE techniques, and the effect of the deposition process and subsequent annealing on their optical and structural properties was examined through ultraviolet–visible (UV–Vis) spectroscopy and spectroscopic prism coupling, and by micro-thermal analysis, respectively. The $Ge_{23}Sb_7S_{70}$ composition is of particular interest because it is currently being employed as the oxidation-resistant overcladding layer in a number of microresonator-based thin film sensing devices [19]; because of its use in these wave-guiding structures, an accurate assessment of the deposition-induced variations in the optical properties, most importantly the refractive index, is critical for the design and implementation of this material system for these applications. Micro-Raman spectroscopy was used to characterize and compare the structure of the films to each other and to their parent bulk glass. A correlation between the optical and thermal properties and the structure of the films is proposed and the variation of these properties between the bulk and films is discussed in terms of deposition-induced structural changes.

2. Experimental

2.1. Target preparation

$Ge_{23}Sb_7S_{70}$ bulk glasses were prepared for use as targets. The glasses were melted from high-purity elements (Ge: Aldrich 99.999%, Sb: Alpha 99.9% and S: Cerac 99.999%). As described previously [20], starting materials were weighed and batched into fused silica ampoules inside a nitrogen-purged glove box. Prior to sealing and melting, the ampoule and batch were pre-heated to 100 °C, while under high vacuum, for 4 h to remove surface moisture from the quartz ampoule and the batch raw materials. The ampoule was then sealed with a gas–oxygen torch and heated to 975 °C to melt for 15–24 h, depending on the mass of the batch. A rocking furnace was used for melting in order to increase the homogeneity of the resultant glass. Once fully homogenized, the melt-containing ampoule was air–quenched to room temperature. To avoid fracture of the tube and glass ingot, the ampoules were subsequently returned to the furnace for annealing for 15 h at 40 °C below the glass transition temperature (T_g).

Deposition of the bulk glass was performed using either small, unpolished bulk pieces for thermal evaporation or polished target samples (2 cm in diameter by 3 mm thickness) for pulsed laser deposition. Thermal evaporation of powdered bulk glass targets on microscope slides were carried out with a base pressure $<10^{-6}$ torr in an Edwards E306A single-source evaporator. During evaporation, the current and voltage on a tantalum boat containing the bulk glass target were monitored in order to establish the vapor pressure in the chamber needed to maintain a constant evaporation rate of 18 Å s^{-1}. The substrate upon which the film was deposited was maintained at 25 °C throughout the deposition, and the films were not annealed following deposition. Thermal evaporation deposition conditions were optimized with respect to the optical performance of the deposited films (e.g. thickness uniformity, surface quality, particle count and adhesion to substrate) and are extremely repeatable, as shown in the device performance demonstrated in Ref. [20]. However, while these TE deposition conditions ensure the film is of high optical quality, this process leads to a slight deviation in the film composition as compared to that of the bulk glass, as discussed below. Pulsed laser deposition using a polished glass target was carried out using a mode-locked Nd:YVO_4 laser [21] operating at the third harmonic (355 nm). The system delivered a total of ~5 W of optical energy to the target. The base pressure in the PLD deposition chamber was 5.0×10^{-7} torr. The substrate upon which the film was deposited was maintained at 25 °C throughout the deposition, and the films were not annealed following deposition.

The chemical composition of the parent bulk glass and the as-deposited thin films were examined using a Hitachi model 3400 scanning electron microscope (SEM), equipped with an energy-dispersive spectroscopy (EDS) accessory. Electron micrographs and EDS spectra, with sensitivity

factors for each element obtained by comparison with measurements of known reference materials, were obtained at 20 keV in variable pressure mode (typically 0.225 torr) in order to avoid sample charging.

The thermal properties of the films (still attached to the substrate) were measured using a TA Instruments model 2990 micro-thermal analyzer (μTA). This μTA device incorporates a U-shaped Pt/Rh Wollaston wire (~5 μm dia.) probe which functions simultaneously as both a resistive heater and resistive temperature detector. The probe is placed on an AFM scanner which allows high precision imaging in two dimensions. A temperature-controlled stage (held at 27 °C) was used to prevent temperature drift errors caused by changes in ambient measurement conditions. The probe penetration temperature, T_p, of the investigated glasses was measured by positioning the thermal probe at the surface of the glass (under a low, constant force), using a heating rate of 10 °C s^{-1}. Upon heating, an upward displacement of the probe was initially seen, caused by the thermal expansion of the film/substrate and of the probe itself. At some maximum, material-specific temperature, the upward motion of the probe ceased and the probe began to penetrate the specimen's surface, yielding a marked change in both the slope of the sensor position and of the power signal, as seen in Fig. 1, which shows the thermogram of the PLD film, taken as an example. The onset point of the slope change (as determined by the change in the first derivative of the signal) was defined as T_p. At 10 °C s^{-1} the accuracy in determining the onset temperature T_p was estimated to be ±10 °C. This large uncertainty is related to the high sensitivity of the micro-thermal analyzer to fluctuations associated with subtle system vibration and air currents (despite the probe/specimen enclosure). As explained in detail in Ref. [21], by raising the heating rate, the elapsed time of the experiment is shortened below the time-scale of these fluctuations, resulting in significantly increased stability.

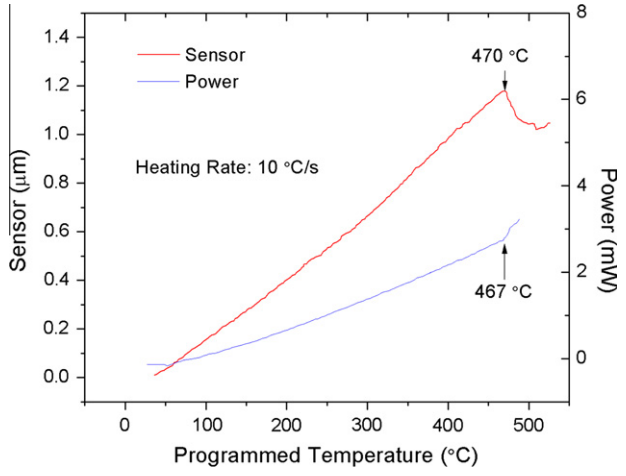

Fig. 1. Sample thermogram of the PLD film produced using micro-thermal analysis at a heating rate of 10 °C s^{-1}. The left axis shows the relative position of the sensor probe head as temperature increases: the maximum at 470 °C indicates the temperature at which the glass network softens. The right axis shows the power output of the probe and the slope change indicates a change in the heat capacity of the material.

The refractive index dispersion of the bulk glass was measured using a custom-modified prism coupling system based on a commercial instrument (Metricon model 2010). To perform the measurement of refractive indices at longer wavelengths, the instrument was modified by the addition of several laser sources, including a 1.547 μm fiber-coupled laser, a 3.391 μm He–Ne laser, a 5.35 μm quantum cascade laser (Maxion Technologies) and a tunable CO_2 laser providing several wavelengths in the 9.3–10.6 μm range. Additional modifications include the use of a GaP prism, in order to provide an appropriate refractive index and transparency range, and an uncooled MCZT detector (Vigo Systems), suitable for wavelengths greater than 2 μm. The IR optical input was modulated at 1.5 kHz using an optical chopper, and the signal was recovered using a current preamplifier (Stanford) and a lock-in amplifier (Princeton), the output of which was fed directly into the commercial instrument controller. The refractive index was calculated with an accuracy of ±0.0005 for each wavelength using the method proposed by Kirsch [22]. A full description of the instrumental design will be published separately.

The refractive index of the thin films was measured at 633 nm using the prism coupling method. Their refractive index dispersion was calculated from UV–Vis–near infrared (NIR) transmission spectra using Swanepoel's method [23]. The transmission spectra were recorded at room temperature using a Perkin Elmer Lambda 900 spectrophotometer over a wavelength range of 300–1500 nm.

The micro-Raman spectra for the parent bulk glass and deposited films were recorded using a Kaiser Hololab 5000R Raman spectrometer with a Raman microprobe attachment. This system has a typical resolution of 2–3 cm^{-1} at room temperature and uses a backscattering geometry. The system consists of a holographic notch filter for Rayleigh rejection, a microscope equipped with ×10, ×50 and ×100 objectives (the latter allowing Raman spectra to be collected from spot sized down to 5–7 μm) and a CCD detector. A 785 nm NIR semiconductor laser is used for excitation with an incident power of approximately 2 mW. The use of a 785 nm source with a low power was specific to our study in order to avoid any photo-structural changes which the laser beam might induce in the samples during measurement. Three measurements per sample were compared and averaged, and the resulting spectra are reported.

3. Results

The aim of this study was to compare the thermal, optical and structural properties of $Ge_{23}Sb_7S_{70}$ thin films deposited by TE and PLD techniques to each other and to those of their parent bulk glass, and to evaluate the effect of annealing on those properties.

$Ge_{23}Sb_7S_{70}$ thin films were deposited onto borosilicate microscope slides, and microscopic inspection using the

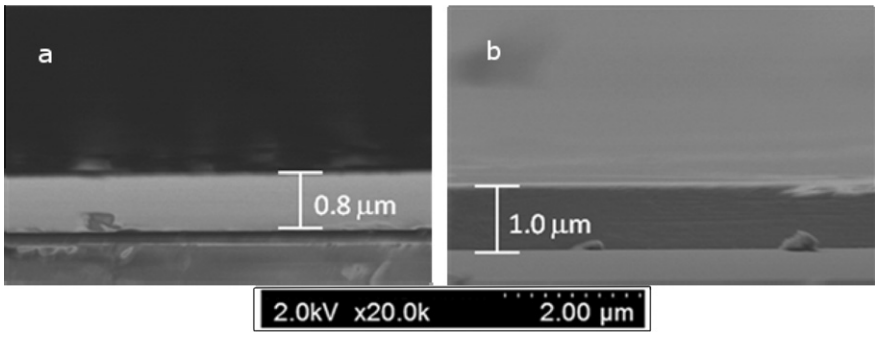

Fig. 2. SEM images of edge of TE (a) and PLD (b) films (magnification = × 20,000). These images were used to estimate the film thicknesses of 0.8 and 1.0 μm for TE and PLD respectively. The images show good uniformity and a homogeneous microstructure.

Table 1
Composition variation between bulk glass and thin films, as measured via EDS.

Sample	Ge (±1 at.%)	Sb (±1 at.%)	S (±1 at.%)
Bulk glass	23	7	70
TE film	23	11	66
PLD film	23	7	70

SEM indicated a uniform, homogeneous morphology, as seen in the electron micrographs taken of the films cross-sections, presented in Fig. 2. The thicknesses of the as-deposited TE (a) and PLD (b) films were found to be 0.80 and 1.0 ± 0.1 μm, respectively. Neither film presented any obvious signs of local compositional variation nor phase separation, as evident from uniform elemental maps obtained using energy dispersive spectroscopy (EDS) both across several 1 mm^2 areas of sample surface and along the cross-section. While the PLD film showed a composition identical to that of the parent bulk glass, within the error of the measurement (±1 at.%), the composition of the TE film showed a slight variation in the Sb/S ratio and was consistently found to be $Ge_{23}Sb_{11}S_{66}$. Sensitivity factors for each element were obtained by comparison with measurements of known reference materials in the instrument's software. The results of the EDS measurements are presented below in Table 1.

The probe penetration temperatures, T_p, of the TE and PLD films are 468 and 470 ± 10 °C respectively, when measured at a scan rate of 10 °C s^{-1}. In comparison, the T_p of the parent bulk glass is 412 ± 10 °C measured at the same rate. The T_p of the bulk and thin film are thought to be very close to the bulk glass dilatometric softening point, T_s, which nominally corresponds to a viscosity of $10^{8.6}$ Pa s [25]. Furthermore, any differences between these viscosity points in bulk glass and thin film materials may be related to changes in the glass structure induced during the deposition process, itself induced by the different thermal histories experienced by the two glass networks. It was found the annealing of the films produced no change in T_p for either film within the error of the measurement (±10 °C).

The UV–Vis–NIR transmission spectra of the as-deposited and annealed films are presented in Fig. 3. As can be seen from the figure, a periodic variation in the transmission

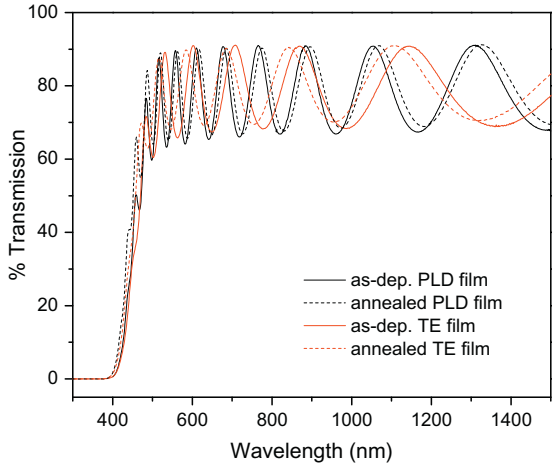

Fig. 3. Transmission spectra of TE and PLD films on glass substrates were used to calculate the absorption coefficient and refractive index dispersion using the method of Swanepoel.

spectra as a function of wavelength is observed, which is caused by interference between multiple reflections at the two surfaces of the film. The magnitude and spacing of this modulation are influenced by the film thickness and refractive index. The fringe strength of the PLD deposited film is slightly greater than that of the TE film, and annealing alters the interference pattern, suggesting a change in refractive index and/or thickness upon annealing. In order to act as a point of reference, the refractive index dispersion curve of the bulk glass was measured using a custom-modified Metricon prism coupling system, for the first time to our knowledge, over the wavelength range of 0.6–10.6 μm, and is presented in Fig. 4. A Sellmeier dispersion curve was generated from this data for the purpose interpolating between the measured wavelengths, and was found to follow the form:

$$n^2 = 1 + \frac{3.252\lambda^2}{(\lambda^2 - 0.2263^2)} + \frac{0.3119\lambda^2}{(\lambda^2 - 0.1989^2)} + \frac{3.0245\lambda^2}{(\lambda^2 - 44.93^2)} \quad (1)$$

In order to calculate both the thickness and index of a thin film using this technique, multiple modes must be coupled into the film [22]. This requirement restricts practical

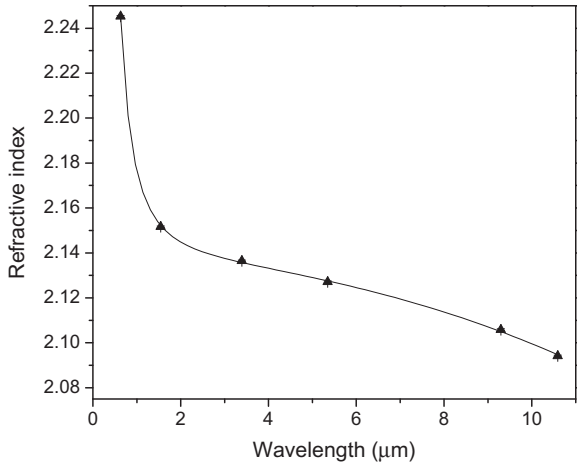

Fig. 4. Refractive index values (±0.0005), as measured using infrared spectroscopic prism coupling, fitted with a Sellmeier dispersion curve.

application to wavelengths shorter than the optical thickness, and limits the possibility of IR index measurements employing the prism coupling method to relatively thick films.

Due to the limitation of prism coupling in measuring film index in this case, the well-known method of Swanepoel [23] was employed to calculate the thickness and refractive index dispersion of the films from their transmission spectra. The thicknesses of the as-deposited films obtained from the fitting process corresponded to those measured with the SEM, and the refractive index dispersion data for the films is compared with that of the bulk glass in Fig. 5a. It can be seen that the index of both films is higher than that of the bulk glass, and that the index of the PLD film is higher than that of the TE film. Moreover, upon annealing, the thickness of the films increases with a corresponding decrease in the refractive index. Thus, the index of both films becomes more bulk-like upon annealing.

As these glasses are expected to show an indirect band gap transition, the absorption coefficient (α) is expected to vary with the square of the photon energy ($h\nu$) according to the Tauc power law:

$$\alpha h\nu = B(h\nu - E_g)^2 \quad (2)$$

where B is the slope of the Tauc edge and E_g is the band gap energy [24]. By performing a linear regression of the variation of $(\alpha h\nu)^{1/2}$ vs. $h\nu$, as shown[1] in Fig. 5b, the band gap may the determined from the point at $\alpha = 0$. As can be seen from the figure, the band gap of the TE film is lower (red-shifted) than that of the PLD film, and the band gap of both films becomes larger (blue-shifted) upon annealing. This result is consistent with Kramers–Kronig analysis of the refractive index dispersion, though it was not possible to directly compare the band gap of the films to the bulk due to the large difference in thickness (optical path length). Also based on Kramers–Kronig analysis, it may be expected that the band gap of the bulk glass lies at higher energy than those of the films, which suggests that the band-gap of the films, like the refractive index, becomes more bulk-like upon annealing.

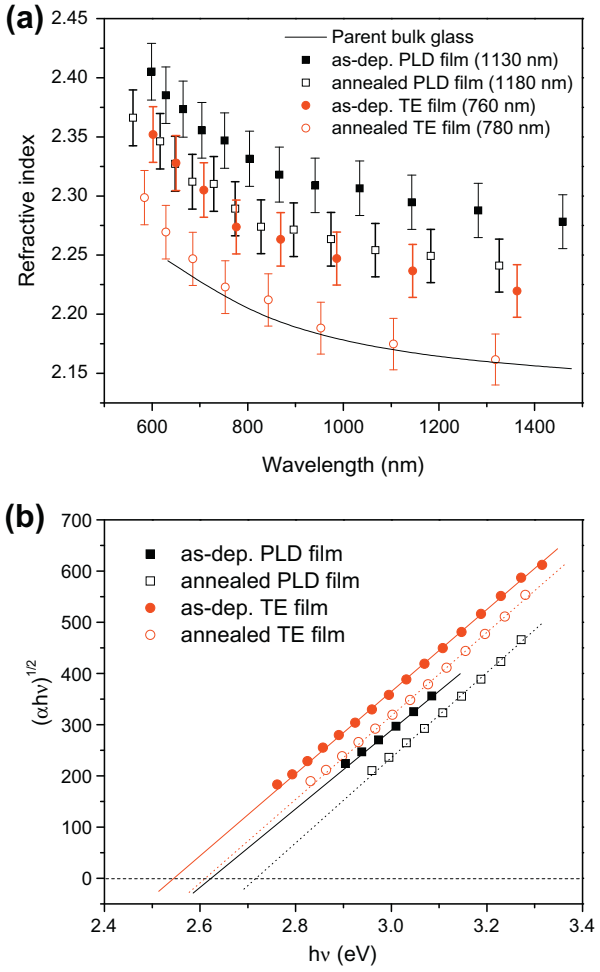

Fig. 5. (a) Refractive index dispersion for the various films as estimated from fitting of the transmission spectra in Fig. 3, using Swanepoel's method. The refractive index of the bulk glass calculated from its Sellmeier dispersion curve (Fig. 4) is presented for comparison (solid line). (b) Calculation of the band gap energy, E_g, of the films from the transmission spectra shown in Fig. 3.

The Raman spectra of the films, shown in Fig. 6, appear to be similar to that of the bulk glass, but with notable changes in the intensity of bands near 250, 360 and 475 cm^{-1}, as well as a shift of the main band to lower wavenumbers. Explained in detail elsewhere [19], the main Raman band, centered near 330 cm^{-1}, is formed primarily by two superimposed bands at 340 and 330 cm^{-1}, which correspond to the A_1 mode of "isolated" GeS_4 [25] and corner-shared (CS) $GeS_{4/2}$ [26] tetrahedral units respectively. A band near 300 cm^{-1}, also present, is attributed to the E_1 mode of $SbS_{3/2}$ pyramids [27]. The shoulder of the main band at higher wavenumbers is formed by three bands near 360, 410 and 425 cm^{-1}, respectively attributed to the A_1^c "companion" mode of $GeS_{4/2}$ in the form of edge-shared

[1] For interpretation of color in Fig. 5, the reader is referred to the web version of this article

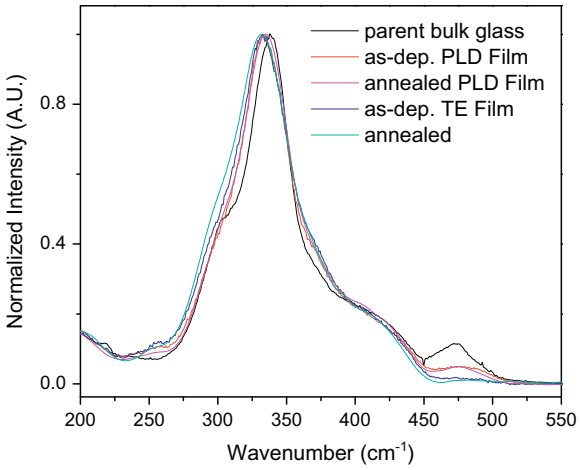

Fig. 6. Micro-Raman spectra of Bulk glass and of TE and PLD films ($\lambda_{exc} = 785$ nm). While the structures of the bulk and films are similar, the spectra show small but significant differences, indicating changes in structure which are dependent on the deposition process.

(ES) $Ge_2S_2S_{4/2}$ bi-tetrahedra [26], the anti-symmetric stretch (F_2) of $GeS_{4/2}$ units [26] and the T_2 motion of bridging S atoms between CS tetrahedra in $S_{3/2}Ge–S–GeS_{3/2}$ [25]. These units are illustrated in Fig. 7 for reference, and the important modes are enumerated in Table 2.

4. Discussion

The property differences between the bulk glass and the thin films, as well as the response of the films during annealing, may be better understood through examination of their Raman spectra. It is possible to describe the glass network in terms of molecular units (centered on the cationic constituents) and to calculate their relative concentrations from the composition of the glass. However, as we will show, the situation in this particular glass is somewhat complex. Based on interpretation of the Raman spectra, the network appears to be composed of $SbS_{3/2}$ units and $GeS_{4/2}$ units which, due to the low Sb content, form the majority of the network. Due to the stoichiometric excess of S, a large number of S–S homopolar bonds are also expected, such as Ge–S_n–Ge bridges, where S_n is a S–S chain (with $n \geqslant 2$) functioning as a bridge between neighboring Ge centres. A Ge–S tetrahedral unit may therefore be expected to be tied into the network through four CS

Table 2
Assignments of some vibrational modes seen in the Raman spectrum of $Ge_{23}Sb_7S_{70}$.

Raman shift (cm^{-1})	Assignment	Refs.
330	A_1 symmetric stretching mode of CS $GeS_{4/2}$ units	[26]
340	A_1 symmetric stretching mode isolated GeS_4 units	[25]
370	T_2 mode $Ge_2S_2S_{4/2}$ units (A_1^c mode ES $GeS_{4/2}$)	[26]
400	Anti-symmetric stretch of $GeS_{4/2}$	[25,26]
425	Stretching motion of $S_{3/2}Ge–S–GeS_{3/2}$ bridges	[25]
290	Asymmetric stretch of $SbS_{3/2}$ units	[34]
475	A_1 symmetric breathing mode of S_8 rings	[27,35]
490	S–S stretch in S_n bridging chains ($n \geqslant 2$)	[27,35]

sulfur atoms (as in $GeS_{4/2}$), or through as many as 4 S_n bridges (as in GeS_4), which is termed "isolated".

Because the A_1 mode of the corner-shared $GeS_{4/2}$ units is found at 330 cm^{-1} and that of isolated GeS_4 is found at 340 cm^{-1}, the main band should in fact be formed by the overlap of the A_1 modes of five different unit types (with between 0 and 4 S_n bridges connecting the Ge centre to the network). This overlap would form a single broad band, the centre of which is expected to shift with a change in the average number of S_n bridges. In order to simplify our interpretation, we have chosen to focus our analysis on only to the two extremes of fully isolated GeS_4 and fully S-shared $GeS_{4/2}$ units, understanding that the relative numbers of these idealized units actually represent the relative numbers of Ge–S–Ge and Ge–S–S–Ge bridges. It should also be noted that it is possible for neighboring tetrahedral units to share two S atoms, forming a shared edge (as in $Ge_2S_2S_{4/2}$), which is indicated by the GeS_4 "companion" (A_1^c) mode at 360 cm^{-1}.

Finally, it should be noted that some S_8 molecular rings are present in the glass, as indicated by Raman intensity near 495 cm^{-1}; however, the exact concentration of S_8 rings, or average S_n chain lengths, cannot be known without precise information regarding their relative scattering cross-sections. It is important to note a particular difficulty caused by this uncertainty, which is the potential interconversion of S chains/rings to S–S bridges. For example, in the following reaction:

$$\text{Ge–S–Ge} + \text{Ge–S–S–S–Ge} \rightarrow \text{Ge–S–S–Ge} + \text{Ge–S–S–Ge} \quad (3)$$

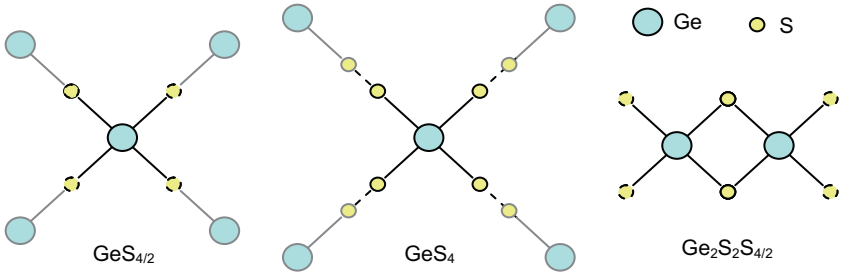

Fig. 7. Molecular units of interest in the analysis of the Raman spectra.

the total number of S–S homopolar bonds (two) remains unchanged, while the number of $GeS_{4/2}$ units would be reduced in order to form more GeS_4 units and S_n chains (but with a shorter average length). The same type of interconversion may also be expected for S_8 rings. The potential for significant impacts to the glass properties becomes apparent by examining the average coordination number (CN) of the various network units. In accordance with the mean-field rigidity theory developed by Phillips and Thorpe [28–30], the amount of residual stress frozen into an amorphous material may be predicted from the average of the coordination numbers ($\langle CN \rangle$) of the units composing the glass network. A network composed of both $GeS_{4/2}$ units ($\langle CN \rangle = 2.67$) and long S_n chains ($\langle CN \rangle = 2$) may be seen as being segregated into over-constrained (stressed rigid) and under-constrained (floppy) regions, while recombination of these into a GeS_4-based network ($\langle CN \rangle = 2.4$) would be considered optimally constrained (isostatically rigid). Intrinsic phase separation of over-constrained Ge-based glasses into regions of higher and lower coordination over nanometer scales has been demonstrated by Mamedov et al. [31]. Moreover, the presence of the S_8 rings ($\langle CN \rangle = 2$), which are not connected to the glass network, would be expected to increase the coordination of the remaining network at any given composition. Thus, alteration of the bond statistics can give topologically different glass networks, which may also be expected to give rise to different thermal and optical properties. This type of conversion between disulfide bridges and S_8 rings has previously been observed during laser irradiation of this composition and is reported in detail elsewhere [32,33].

With regard to comparing the structure of the bulk glass and thin films, one can observe slight differences between the Raman spectra of the bulk glass and as-deposited films, including a shift of the main band of the films to lower wavenumber, an increased intensity for the bands near 360 and 425 cm^{-1} and a decreased intensity at 475 cm^{-1}. These changes indicate a conversion of GeS_4 units (in the bulk) to CS and ES $GeS_{4/2}$ units (in the films), with a corresponding reduction in S–S bonds, and appear to be more significant in the case of the TE film than in the PLD film. Together, these findings suggest that the films have a more tightly bonded structure than the parent bulk glass. Such an effect may be attributed to the formation of small, tightly interconnected molecular fragments such as $Ge_2S_2S_{4/2}$ in the gas phase or plasma plume during TE or PLD, respectively, which become frozen into the film due to the relatively high quench rate during deposition. Evidence of these more tightly bonded structures is seen in the increase in the shoulder of the main band near 370 cm^{-1}. It may further be expected that such a glass network should possess a higher density, explaining both the increased probe penetration temperatures and increased refractive indices observed for the as-deposited films, as compared to the bulk glass.

The additional observation of a small band near 250 cm^{-1}, corresponding to Ge–Ge bonds in the films but not present in the bulk glass, further supports the idea of rapid quenching, as these bonds are not thermodynamically preferred. It is commonly believed that such bonding defects form mid-gap states, leading to the observed red shift of the optical band gap in the as-deposited films. Kramers–Kronig analysis predicts that such an effect should further serve to increase the refractive index of the films relative to the bulk glass. As a final note, the slight compositional change during deposition of the TE film seems to produce a few additional effects, such as the possession of a slightly lower refractive index compared to the PLD film, while also having a relatively smaller (red-shifted) band gap. This suggests that both density and band gap differences play a role in the deposition-induced refractive index variation. This compositional difference is reflected in the increased intensity near 300 cm^{-1}, related to SbS_3 units, and by the very low S–S bond content (475 cm^{-1}) of the TE film, as this film possesses only a 3% stoichiometric excess of S, compared to 13% for the bulk glass.

As may be expected, the annealing process leads to film properties that are more similar to those of the bulk glass, including a blue shift of the band gap and a reduction in the refractive index. These may both be linked to a reduction in Raman intensity near 250 and 490 cm^{-1}, which is attributed to the partial removal of Ge–Ge bonds and the corresponding decrease in the S–S bond content. Interestingly, the main band of the PLD film shifts to a higher wavenumber during annealing, indicating a larger number of GeS_4 units, while that of the TE film shifts to a lower wavenumber; however, both films become thicker and have a lower refractive index after annealing, suggesting that the density of both films decreases. This difference in behavior is likely due to the slight compositional change observed during TE deposition; however, a more thorough examination of the bonding environment around S, for example through X-ray photoelectron spectroscopy (XPS), may allow better understanding of these phenomena.

5. Conclusions

In this paper, we have demonstrated that films with the composition $Ge_{23}Sb_7S_{70}$ can be deposited using TE and PLD techniques. We discussed the effect of the film deposition process on the thermal, optical and structural properties of the glasses. Resulting films were found to have compositions similar to that of the parent glass target. Micro-thermal analysis revealed that the TE and PLD films have similar probe penetration temperatures (T_p), at 468 and 470 ± 10 °C respectively, which are significantly higher than that of the parent bulk glass 412 ± 10 °C, suggesting a more tightly connected network. The refractive indices of the films measured by Swanepoel's method and by ellipsometry are higher than that of the bulk glass as measured by prism coupling, with the unannealed PLD film having the highest index observed in this study.

Using micro-Raman spectroscopy, the films are found to have similar structures to each other, but are not identical to that of the bulk. We explained that the high cooling rate during the film deposition freezes in small, highly interconnected $GeS_{4/2}$ structures, which consequently gives rise to higher T_p and refractive index through changes in the free volume. A slight compositional change during thermal evaporation leads to additional effects of film properties. Annealing of the films was shown to induce a shift to a more bulk-like structure and therefore properties. Understanding these processes is the key for the development of applications such as planar optical sensors.

Disclaimer

This paper has been prepared as an account of work supported by an agency of the United States Government. Neither the United States Government nor any agency thereof, nor any of their employees, makes any warranty, express or implied, or assumes any legal liability or responsibility for the accuracy, completeness or usefulness of any information, apparatus, product or process disclosed, or represents that its use would not infringe privately owned rights. Reference herein to any specific commercial product, process, or service by trade name, trademark, manufacturer, or otherwise does not necessarily constitute or imply its endorsement, recommendation, or favoring by the United States Government or any agency thereof. The views and opinions of authors expressed herein do not necessarily state or reflect those of the United States Government or any agency thereof.

Acknowledgements

Funding is provided by the Department of Energy (Contract # DE-FG52-06NA27502) and by the National Science Foundation (Grant #DMR-0312081 (NSF-EU)). The authors acknowledge support of the Australian Research Council through its Centres of Excellence and Federation Fellow programs, and the Laser Physics Centre (B. Luther-Davies and his group) at ANU, as well as the Centre of Materials Science and Engineering at MIT, for providing film deposition expertise and samples.

References

[1] Seddon AB. J Non-Cryst Solids 1995;184:44.
[2] Fedotova O, Husakou A, Hermann J. Opt Express 2006;14:1512.
[3] Brilland L, Smektela F, Renversez G, Chartier T, Troles J, Nguyen TN, et al. Opt Express 2006;14:1280.
[4] Koudelka L, Frumar M, Pisarcik M. J Non-Cryst Solids 1980;41:171.
[5] Asobe M, Ohara T, Yokohama I, Kaino T. Electron Lett 1996;32:1396.
[6] Vlasov Y, Legin A, Rudnitskaya A, Di Natale C, D'Amico A. Pure Appl Chem 2005;77:1965.
[7] Hu JJ, Tarasov V, Agarwal A, Kimerling L, Carlie N, Petit L, et al. Opt Express 2007;15:2307.
[8] Frumar M, Jedelsky J, Frumarova B, Wagner T, Hrdlicka M. J Non-Cryst Solids 2003;326:399.
[9] Stegeman R, Stegeman G, Delfyett P, Petit L, Carlie N, Richardson K, et al. Opt Express 2006;14:11702.
[10] Harbold JM, Ilday FO, Wise FW, Aitken B. IEEE Photon Technol Lett 2002;14:822.
[11] Ganjoo A, Jain H, Yu C, Song R, Ryan JV, Irudayaraj J, et al. J Non-Cryst Solids 2006;352:584.
[12] Huang CC, Hewak D, Badding J. Opt Lett 2004;12:2501.
[13] Marquez E, Bernal-Olivia AM, Gonzalez-Leal JM, Prieto-Alcon R, Wagner T. J Phys D 2006;39:1793.
[14] Xu J, Almeida RM. J Sol–Gel Sci Technol 2000;19:243.
[15] Yamashita M, Yamanaka H, Wakabayashi H. Solid State Ionics 1996;89:299.
[16] Zakery A, Elliot SR. J Non-Cryst Solids 2003;330:1.
[17] Nazabal V, Cathelinaud M, Shen W, Nemec P, Charpentier F, Lhermite H, et al. Appl Opt 2008;47:114.
[18] Krbal M, Wagner T, Kohoutek T, Nemec P, Orava J, Frumar M. J Phys Chem Sol 2007;68:953.
[19] Carlie N, Musgraves JD, Zdyrko B, Luzinov I, Hu JJ, Singh V, et al. Opt Express 2010;18:26728.
[20] Petit L, Carlie N, Adamietz F, Couzi M, Rodriguez V, Richardson KC. Mater Chem Phys 2006;97:64.
[21] Luther-Davies B, Kolev VZ, Lederer MJ, Madsen NR, Rode AV, Giesekus J, et al. Appl Phys A 2004;79:1051.
[22] Kirsch ST. Appl Opt 1981;20:2085.
[23] Swanepoel R. J Phys E Sci Instrum 1983;16:1214.
[24] Tauc J. Amorphous and liquid semiconductors. New York: Plenum; 1974.
[25] Julien C, Barnier S, Massot M, Chbani N, Cai X, Loireaulozach AM, et al. Mater Sci Eng B 1994;22:191.
[26] Mei Q, Saienga J, Schrooten J, Meyer B, Martin SW. J Non-Cryst Solids 2003;324:264.
[27] Frumarova B, Nemec P, Frumar M, Oswald J, Vicek M. J Non-Cryst Solids 1999;256:266.
[28] Phillips JC. J Non-Cryst Solids 1979;34:153.
[29] He H, Thorpe MF. Phys Rev Lett 1985;54:2107.
[30] Thorpe MF. J Non-Cryst Solids 1983;57:355.
[31] Mamedov S, Georgiev DG, Qu T, Boolchand P. J Phys Condens Matter 2003;15:2397.
[32] Anderson T, Petit L, Carlie N, Choi J, Hu J, Agarwal A, et al. Opt Express 2009;16:20081.
[33] Petit L, Carlie N, Anderson T, Couzi M, Choi J, Richardson M, et al. Opt Mater 2007;29:1075.
[34] Kamitsos EI, Kaptoutsis JA, Culeac IP, Iovu MS. J Phys Chem B 1997;101:11061.
[35] Kincl M, Tichy L. Mater Chem Phys 2007;103:78.